Production of hydrogen isotopes and charged pions in p (3.5 GeV) + ^{93}Nb reactions

R. Abou Yassine,[6,14] O. Arnold,[10,9] M. Becker,[11] P. Bergmann,[5] A. Blanco,[1] C. Blume,[8] M. Böhmer,[10] N. Carolino,[1] L. Chlad,[15,*] P. Chudoba,[15] I. Ciepał,[3] J. Dreyer,[7] W. A. Esmail,[5] L. Fabbietti,[10,9] P. Fonte,[1,†] J. Friese,[10] I. Fröhlich,[8] T. Galatyuk,[6,5] J. A. Garzón,[16] M. Grunwald,[17] M. Gumberidze,[5] S. Harabasz,[6] C. Höhne,[11,5] F. Hojeij,[14] R. Holzmann,[5] H. Huck,[8] M. Idzik,[2] B. Kämpfer,[7,‡] B. Kardan,[8] V. Kedych,[6] I. Koenig,[5] W. Koenig,[5] M. Kohls,[8] G. Korcyl,[4] G. Kornakov,[17] F. Kornas,[6,5] R. Kotte,[7] W. Krueger,[6] A. Kugler,[15] T. Kunz,[10] R. Lalik,[4] L. Lopes,[1] M. Lorenz,[8] A. Malige,[4] J. Markert,[5] V. Metag,[11] J. Michel,[8] A. Molenda,[2] C. Müntz,[8] L. Naumann,[7] K. Nowakowski,[4] J.-H. Otto,[11] Y. Parpottas,[12] M. Parschau,[8] V. Pechenov,[5] O. Pechenova,[5] J. Pietraszko,[5] A. Prozorov,[15,*] W. Przygoda,[4] K. Pysz,[3] B. Ramstein,[14] N. Rathod,[4] A. Rost,[6,5] A. Rustamov,[5] P. Salabura,[4] N. Schild,[6] E. Schwab,[5] F. Seck,[6] U. Singh,[4] S. Spies,[8] M. Stefaniak,[17,5] H. Ströbele,[8] J. Stroth,[8,5] C. Sturm,[5] K. Sumara,[4] O. Svoboda,[15] M. Szala,[8] P. Tlusty,[15] M. Traxler,[5] H. Tsertos,[13] V. Wagner,[15] A. A. Weber,[11] C. Wendisch,[5] H. P. Zbroszczyk,[17] E. Zherebtsova,[5,§] and P. Zumbruch,[5]
(HADES Collaboration),
B. Kamys,[4] and S. Sharma[4]

[1]*LIP-Laboratório de Instrumentação e Física Experimental de Partículas, 3004-516 Coimbra, Portugal*
[2]*AGH University of Science and Technology, Faculty of Physics and Applied Computer Science, 30-059 Kraków, Poland*
[3]*Institute of Nuclear Physics, Polish Academy of Sciences, 31342 Kraków, Poland*
[4]*Smoluchowski Institute of Physics, Jagiellonian University of Cracow, 30-059 Kraków, Poland*
[5]*GSI Helmholtzzentrum für Schwerionenforschung GmbH, 64291 Darmstadt, Germany*
[6]*Institut für Kernphysik, Technische Universität Darmstadt, 64289 Darmstadt, Germany*
[7]*Institut für Strahlenphysik, Helmholtz-Zentrum Dresden-Rossendorf, 01314 Dresden, Germany*
[8]*Institut für Kernphysik, Goethe-Universität, 60438 Frankfurt, Germany*
[9]*Excellence Cluster 'Origin and Structure of the Universe', 85748 Garching, Germany*
[10]*Physik Department E62, Technische Universität München, 85748 Garching, Germany*
[11]*II. Physikalisches Institut, Justus Liebig Universität Giessen, 35392 Giessen, Germany*
[12]*Department of Mechanical Engineering, Frederick University, 1036 Nicosia, Cyprus*
[13]*Department of Physics, University of Cyprus, 1678 Nicosia, Cyprus*
[14]*Laboratoire de Physique des 2 infinis Iréne Joliot-Curie, Université Paris-Saclay, CNRS-IN2P3., F-91405 Orsay, France*
[15]*Nuclear Physics Institute, The Czech Academy of Sciences, 25068 Rez, Czech Republic*
[16]*LabCAF. F. Física, Univ. de Santiago de Compostela, 15706 Santiago de Compostela, Spain*
[17]*Warsaw University of Technology; Faculty of Physics, 00-662 Warsaw, Poland*

(Received 23 January 2023; accepted 14 August 2023; published 4 December 2023; corrected 1 July 2024)

The double-differential production cross sections $d^2\sigma/d\Omega dE$ for hydrogen isotopes and charged pions in the reaction of $p + {}^{93}$Nb at 3.5 GeV proton beam energy have been measured by the high-acceptance dielectron spectrometer (HADES). Thanks to the high acceptance of HADES at forward emission angles and the use of its magnetic field, the measured energy range of hydrogen isotopes could be significantly extended in comparison with the relatively scarce experimental data available in the literature. The data provide information about the development of the intranuclear cascade in the proton-nucleus collisions. They can as well be utilized to study the rate of energy or momentum dissipation in the nuclear systems and the mechanism of elementary and composite particle production in excited nuclear matter at normal density. Data of this type are important also for technological and medical applications. Our results are compared with models developed to describe the processes relevant to nuclear spallation (INCL++) or oriented to probe either the elementary hadronic processes in nuclear matter or the behavior of compressed nuclear matter (GiBUU).

DOI: 10.1103/PhysRevC.108.064902

I. INTRODUCTION

Proton-nucleus collisions are an important tool for the investigation of complex phenomena in strong-interaction physics. In particular, reactions with protons at a beam energy of a few GeV allow us to study spallation reactions in which the target nucleus disintegrates into many smaller fragments and reaction products. A thorough understanding of their underlying mechanisms is relevant, in particular because

*Also at Charles University, Faculty of Mathematics and Physics, 12116 Prague, Czech Republic.
†Also at Coimbra Polytechnic - ISEC, Coimbra, Portugal.
‡Also at Technische Universität Dresden, 01062 Dresden, Germany.
§Also at University of Wrocław, 50-204 Wrocław, Poland.

these reactions are excellent tools for fundamental and applied science [1–5]. One example for an important application of spallation reactions is nuclear waste transmutation in accelerator driven systems (ADSs) [3–10]. They are also crucial for the understanding of the nuclear spallation contribution to nucleosynthesis [11–15], cosmic-ray propagation in the Galaxy [16] or extensive air showers generated by high-energetic cosmic rays [17]. Proton-nucleus collisions also provide a valuable laboratory for the investigation of light nuclei formation in excited nuclear systems [18]. Finally, they serve as an essential baseline measurement for the interpretation of heavy-ion collision data with respect to dense nuclear matter.

A characteristic property of spallation reactions is the abundant emission of neutrons. Due to this fact, it was possible to build efficient sources of neutrons with controlled flux and energy distribution (so-called spallation sources). It is therefore not surprising that neutron production in spallation reactions was intensively studied experimentally, and nuclear models were developed to parametrize neutron angular distributions and energy spectra in interactions of protons with thin and thick targets, cf., e.g., Refs. [19,20]. These models were, however, not able to reproduce satisfactorily the emission of protons and light charged particles like tritium and helium isotopes which may strongly influence the stability of the neutron source. Thus, subsequent experimental [21] and theoretical [22,23] investigations were undertaken for these purposes. Furthermore, the emission of other products in spallation reactions, like pions [24], as well as complex heavy nuclei, were studied both experimentally [25–27] and theoretically [28–31].

In spite of these efforts, there remain problems which are not satisfactorily explained by existing models [32,33]. It is therefore necessary to continue the studies of spallation reactions to gain additional insight in the detailed mechanism of these processes.

According to Serber [34], proton-nucleus collisions proceed in two steps. During the first, the dynamical one, the projectile particle transfers its energy to the nuclear target in a cascade of binary collisions with the target constituents. During this stage, the production and emission of energetic particles is expected. The second step consists of a statistical emission of slow particles from the thermalized remnant of the target nucleus. Such a two-step picture of the reaction agrees well with the angular distributions of observed reaction products, which are found to be isotropic for low-energy products and forward-peaked for high-energy ones. It also agrees with the properties of their energy spectra, which are of Maxwellian shape for small and of exponential shape for large particle energies. However, present day models are not able to quantitatively reproduce the differential [35], as well as the total [30,31] production cross sections of complex particles emerging from spallation reactions. Such effects were observed for all target nuclei starting from light ones, such as, e.g., Ni [36], through intermediate masses such as Ag [33], to heavy ones such as Au [37] nuclei. Therefore, it seems indispensable to reexamine in more detail the emission mechanism of the main products of spallation reactions, such as nucleons and pions. While the production of neutrons was investigated in great detail, because of its technological applications, the proton and pion data are not abundant. Especially data on proton and pion production cross sections measured simultaneously in one experiment are rare. In the last years, such reactions were studied by the HARP (see Ref. [38] and references therein) and HARP-CDP (see Ref. [39] and references therein) Collaborations.

The present investigation yields both the double-differential cross sections for charged pions as well as for hydrogen isotopes produced in collisions of a 3.5 GeV proton beam with a ^{93}Nb target, measured by the HADES Collaboration [40,41]. The experimental data are confronted with the results of two commonly used models (INCL++ [29] and GiBUU [42]).

Our paper is organized as follows: In Sec. II the experimental setup of HADES is described and the parameters of most relevant parts of the detection system are given. Section III presents the analysis procedures applied in order to derive the double-differential cross sections of interest. Various components of experimental uncertainty are discussed as well. In Sec. IV the full set of double-differential cross sections for p, d, t, π^+, and π^- are given. In Sec. V, the verification of the analysis scheme applied in this study is done by a comparison of the current results with examples of similar data available in the literature. Section VI provides the main assumptions of the applied models. Methods of evaluation of the cross sections are presented as well. The comparison of theoretical and experimental results for the currently examined reactions is discussed in Sec. VII. The conclusions about validity of the models in their description of the studied collision dynamics and their predictive power are also given. The summary of the work is presented in Sec. VIII.

II. EXPERIMENTAL SETUP

The high-acceptance dielectron spectrometer (HADES) [40,41] of the Heavy-Ion Research Laboratory (GSI Helmholtz Center für Schwerionenforschung), Darmstadt, Germany is optimized to perform the research with proton, pion, and heavy-ion beams impinging on stationary solid or liquid targets. It provides information about production rates, angular and energy distributions for dileptons, mesons, and baryonic products. The presented results are derived from experimental data where a ^{93}Nb target has been bombarded by 3.5 GeV energy protons [43–50]. For the detection and identification of pions and hydrogen isotopes the most important components of the detection system are target, multiwire drift chambers (MDCs) and scintillating walls called TOF and Tofino. The mutual positions of these detectors are shown in the cross section of the HADES setup presented in Fig. 1.

A segmented solid target of ^{93}Nb has been used in the present experiment. Its diameter was 2.5 mm and its total thickness was 0.45 mm.

The detection system is organized in six identical sectors covering the complete azimuthal angle, except for the magnet coils and providing an acceptance between 18° and 85° in polar angle.

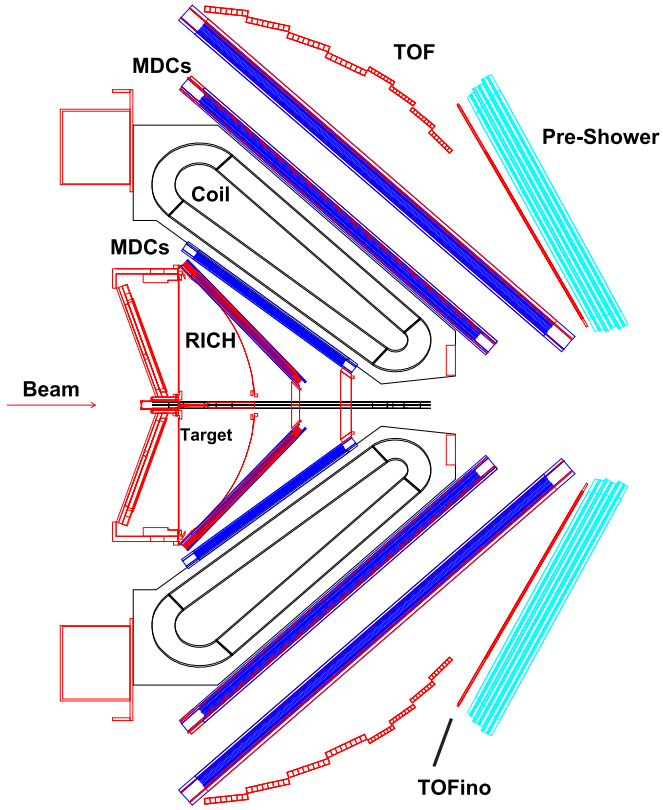

FIG. 1. The cross section of the HADES setup used during the measurement of $p + {}^{93}$Nb reactions at 3.5 GeV. The location of the most important detectors for the measurement of charged pions and hydrogen isotopes is shown relative to the beam axis. The particle identification was based on the dE/dx vs momentum measurements with the multiwire drift chambers (MDCs) and in the TOF-Tofino scintillating walls. The latter were used also as triggering detectors. For more details see the text

The tracking system consists of 24 individual multiwire drift chambers (MDCs). They were filled with argon gas doped by isobutane as a quencher. The MDCs were operated at atmospheric pressure. Their position resolution is $\leqslant$100 μm in polar direction and $\leqslant$200 μm in azimuthal direction. In each detection sector there are two chambers in front and two chambers behind the magnet.

The superconducting toroidal magnet provides a maximal magnetic field of 3.6 T and causes the momentum-dependent bending of the trajectories of charged reaction products. The track reconstruction procedures permit a momentum resolution of $\delta p/p = 4\%$.

Despite of the small effective thickness of the MDC system (0.5% of a radiation length) it is possible to measure the energy loss of charged particles in the detector medium. It is done by means of the measured time-over-threshold [51,52] of a given signal. Taking into account the particle's path length the resulting dE/dx resolution is better than 7%. This allows for the particle identification by means of the specific energy loss.

The TOF and Tofino detectors located at the end of the detection system were intended as stop detectors for the particle time-of-flight measurement. However, given the lack of start detectors during the measurement, they are used as triggering detectors and additional dE detectors only.

The TOF scintillating wall covers polar angles from 44° to 85°. The intrinsic time resolution of the scintillating strip is 150 ps and its position resolution 3 cm. The dE/dx resolution for these scintillators is 4%.

The Tofino covers the polar angles between 18° and 45°. Its timing resolution is 420 ps. Since signals of these detectors are read out only at one side of the scintillating strips, the resulting energy loss resolution is 8%. Tofino has also a worse double hit resolution than TOF.

The analysis of the detected data is accompanied by careful HGeant and HYDRA (Hades system for data reduction and analysis) [41,53] simulations of the response of each part of the detection system including its acceptance, efficiency, tracking, energy loss, and calibration.

The detection system of HADES is described in more detail in Ref. [41].

III. PARTICLE SELECTION AND IDENTIFICATION

A. Particle identification and background subtraction

The particle identification (PID) and the background subtraction utilize the good energy-loss resolution of the MDCs and the TOF-Tofino scintillating walls. A procedure of consecutive cut definitions, ranging from level 1 (mass − momentum distribution) through level 2 (dE/dx_{MDC} vs momentum) to level 3 (dE/dx_{TOF} vs momentum and dE/dx_{Tofino} vs momentum), has been developed.

The mass cut of level 1 provides just a rough separation of the mass ranges of individual species (π^+, p, d, t) in a mass vs momentum plot. Due to the lack of particle velocity measurements during the $p + {}^{93}$Nb data taking, the time of flight (T-o-F) of the selected particle needed for mass calculation was reconstructed by the comparison to the T-o-F of the fastest identified particle of the event. But, as long as the single distributions of reaction products are of interest, the coincidences with other particles have to be disregarded. For this reason the identification based on the mass − momentum dependence for individual particles cannot be utilized for their exact identification in the current analysis. At levels 2 and 3, for each selected bin of laboratory emission angle of 3° width and momentum of 25 MeV/c width, asymmetric Gaussian functions [Eq. (1)], allowing for different widths for low- and high-energy losses, are fit to the dE/dx distributions.

$$f_g\left(\frac{dE}{dx}\right) = \begin{cases} \frac{1}{\sigma_l\sqrt{2\pi}} e^{-\frac{1}{2}\left(\frac{\frac{dE}{dx}-\mu}{\sigma_l}\right)^2} \text{ for } & \frac{dE}{dx} - \mu \leqslant 0 \\ \frac{1}{\sigma_r\sqrt{2\pi}} e^{-\frac{1}{2}\left(\frac{\frac{dE}{dx}-\mu}{\sigma_r}\right)^2} \text{ for } & \frac{dE}{dx} - \mu > 0. \end{cases} \quad (1)$$

The width of the PID cut has been selected according to the value of the total standard deviation of the fitted asymmetric Gaussians: $\sigma = (\sigma_l + \sigma_r)/2$, around the mean value μ of the fitted distribution.

In this way, the two-dimensional (2D) cuts (dE/dx − momentum) for all positively charged reaction products of interest have been created and applied to the raw data in order to select the experimental distributions. The separation of negatively charged pions from other reaction products is

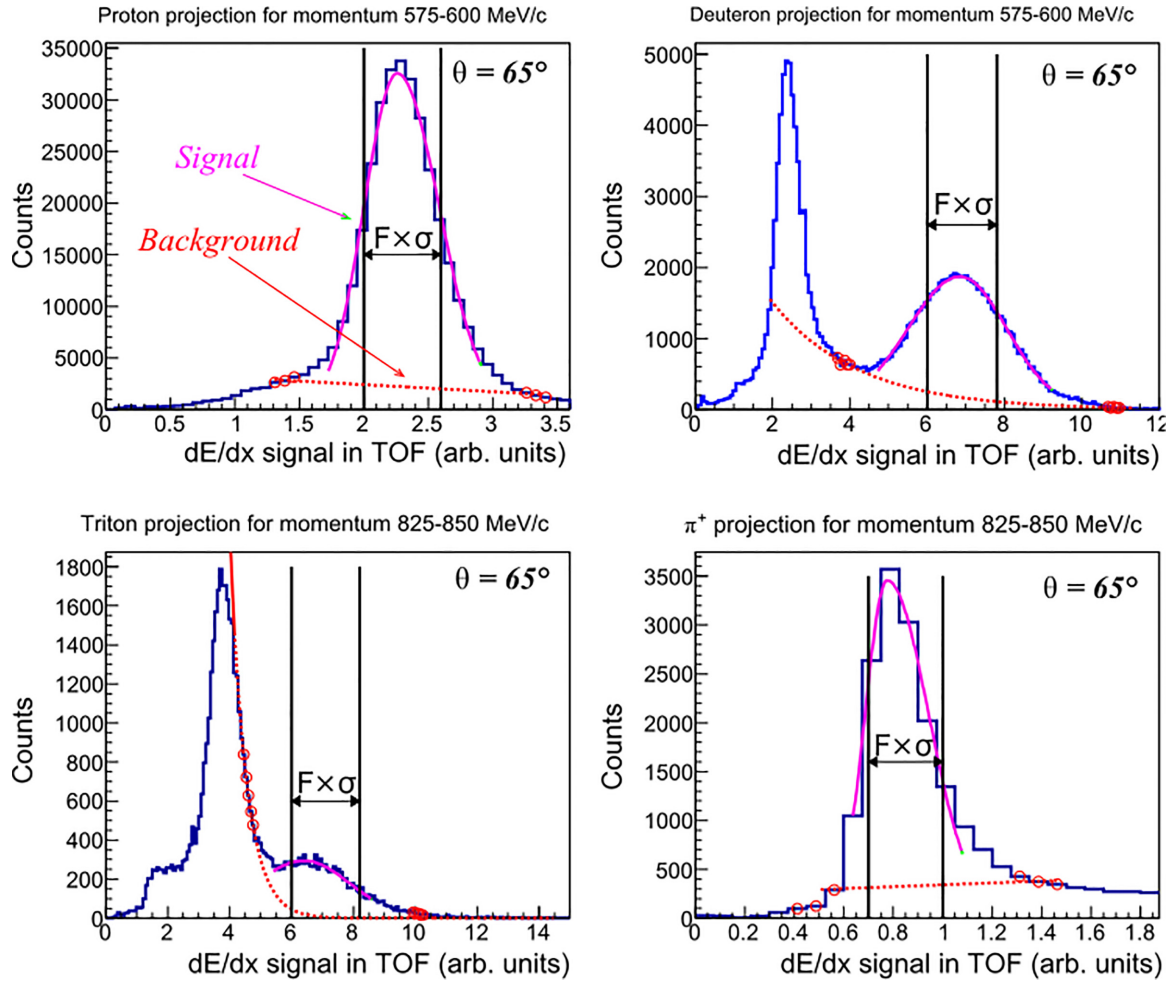

FIG. 2. Examples of the identification of protons (top-left), deuterons (top-right), tritons (down-left), and positively charged pions (down-right) for the emission angle $\theta = 65^\circ$ and the momentum bin of 575–600 MeV/c. The functions fit to the signal peaks are an asymmetrical Gaussian function according to Eq. (1) (continuous purple curves), whereas the underlying background is approximated with a straight line (for protons and π^+) or an exponential function (for deuterons and tritons, dashed and red curves). To the left of the deuteron and triton peaks the contamination by protons or deuterons, respectively, is visible. The PID cuts of various widths equal to $F\sigma$ are applied to the signal component. σ is the width of the respective fitted Gaussian distribution whereas the parameter F takes values between 0.6 and 1.8 (see Sec. III D).

provided by their opposite deflections in the magnetic field. There is no need for an additional particle identification, as contamination of π^- with K^- or e^- is insignificant and disregarded here.

The distributions of selected particles, after their projection onto the $dE/dx_{\mathrm{TOF/Tofino}}$ axis, are fitted with signal and background distributions. It is done again for each momentum bin of 25 MeV/c. The background component originating from misidentified "neighboring" particles is subtracted. Examples of identification of protons, deuterons, tritons and positively charged pions at the emission angle of 65° and for one momentum bin of 575–600 MeV/c are presented in Fig. 2.

The ranges of particle momenta considered for the calculation of cross section have been restricted by the demand that the resulting background-to-signal ratio is not larger than 0.1 for protons and positively charged pions, and 0.6 for deuterons and tritons, extracted in a $\pm 1\sigma$ range of the Gaussian function fit to the signal peak, respectively.

In the HADES apparatus also secondary particles emerging from nontarget material are created. Their contribution to the spectra of primary reaction products is suppressed by the particle selection in the tracking procedure and can therefore be ignored for cross sections of single particles.

B. Determination of efficiency

The overall efficiency has to be taken into account in the absolute normalization of the obtained distributions. Here we define it as the combination of the geometrical detector acceptance (Acc) and efficiency (Eff), where efficiency includes the track reconstruction efficiency, PID efficiency, trigger conditions, and data-acquisition efficiency.

The overall efficiency is calculated using standard simulation tools of HADES - HGeant + HYDRA [41,53]. For generating the initial distributions of charged products in p (3.5 GeV) + ^{93}Nb reactions, the INCL++ model has been

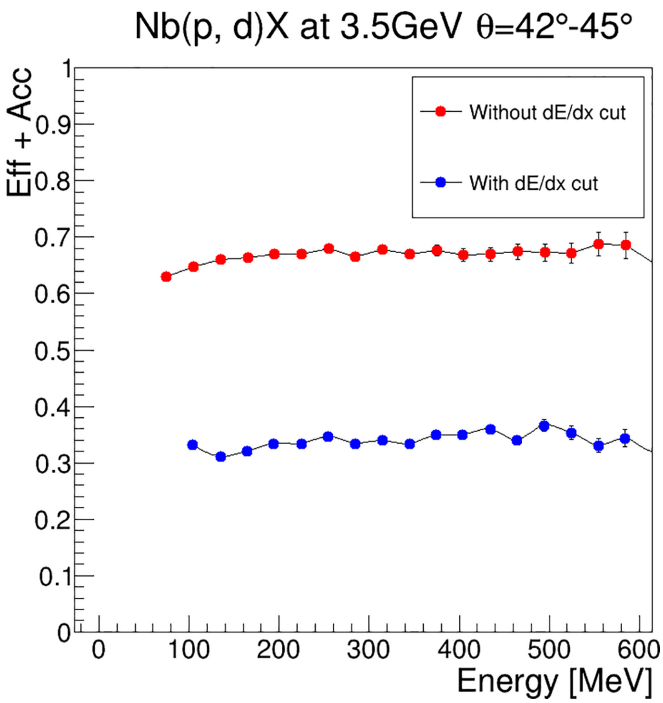

FIG. 3. Example for the combined efficiency and acceptance of deuterons at $42^\circ < \theta < 45^\circ$ laboratory angle. The red dots represent the efficiency obtained without PID cuts, whereas the blue dots show the final efficiency. In this case, the PID cuts were applied to the "real" distributions of deuterons. For details see the text.

applied. It provides realistic yields and distributions of the dominant reaction products.

With the use of the selected event generator the simulated distributions of emission angle θ vs momentum for individual particles are created: the so-called "initial" ones (without taking into account the HADES apparatus) and the "real" ones (with the inclusion of the full response of HADES). The predefined particle identification cuts are applied for the "real" θ vs momentum distributions. By dividing the "real" distribution by the "initial" one, the overall efficiency is calculated, bin-by-bin, for each reaction product of interest. The overall efficiency of the HADES system is angle- and energy-dependent. Thus, the calculated factors are applied to the values of absolute cross section for each emission angle and for each individual energy bin.

Figure 3 shows an example of calculated overall efficiency depending on the energy of detected deuterons for the angular bin of $42^\circ < \theta < 45^\circ$, before and after application of the PID cut to the "real" distribution.

In the present studies, the possible modification of overall efficiency for purely inclusive spectra due to contribution of secondary particles is solved by tracking procedures. The secondaries registered in the triggering detectors create a trigger bias. For the calculation of the overall efficiency, the secondary particles from events generated by INCL++ are "created" by HGeant and effectively tracked by HYDRA back to their vertices. Those not originating from the target are suppressed. This is sufficient for a reliable determination of efficiency by dividing the "real" by "initial" distribution.

The possible bias due to the trigger condition, requiring at least three charged particles registered in TOF-Tofino walls, on the overall efficiency for single spectra is taken into account in the simulations of the "real" distributions with the use of the event generator, HGeant and HYDRA. Thus, the so-called trigger bias on the single spectra does not need to be treated separately.

C. Calculation of cross section

The recorded multiplicity has been calculated for each particle of interest and for each selected energy and angular bin by subtracting the background from the signal distribution and by integrating the differences. The obtained numbers were corrected by the calculated overall efficiency (efficiency $\times$ acceptance) values. For the calculation of the absolute value of the cross sections the normalization factor derived in the former analysis of HADES π^- data has been used [44,54,55]. This normalization factor was obtained by interpolating known pion production cross sections [56–59]. As a result of this interpolation we determine a total reaction cross section of $\sigma_{p\mathrm{Nb}} = 848 \pm 127$ mb. A detailed description of the procedure is given in Ref. [55].

D. Uncertainties

The statistics of the collected data is very high. The total number of analyzed events amounts to about 10^8. For each energy bin of the presented data the statistical error is negligible and is therefore not shown in the plots.

The contributions to the systematic uncertainties are

(i) uncertainty of particle identification;
(ii) uncertainty of overall efficiency;
(iii) differences of the response of individual sectors of the HADES detection system;
(iv) uncertainty of the absolute normalization factor.

Only the last component of the systematic error is independent of phase space and amounts to 15%. This was established in former analyses of HADES pion spectra from p (3.5 GeV) + ^{93}Nb [44] and their comparison to similar results by the HARP-CDP collaboration [55]. Other components are energy and emission angle dependent, and will be shortly discussed below.

1. Particle identification

Due to the lacking mass identification based on the T-o-F information, the deconvolution of the signal and background tracks is based only on the specific energy-loss method. The resolving power of this approach is limited and varies with the energy of particles searched for. To study the level of signal or background misidentification, various widths of identification cuts have been used. The applied cut widths were calculated by multiplication of the standard deviation σ of the fitted asymmetrical Gaussian function by factors F equal to 0.6, 0.8, 1.0, 1.2, 1.5, 1.8 (cf. Fig. 2). For each of the applied cut widths, the quantity of the signal counts is calculated by the subtraction of the background contribution from the signal contribution. The standard deviation of the average of

all obtained results for the given particle, emission angle, and energy bin is assigned as the systematic uncertainty of the PID procedure. For protons this component of the systematic uncertainty does not exceed 5% for almost the complete energy range. The largest values of 12% appear for the highest energies for tritons.

2. Efficiency

Since the method of overall efficiency calculations consists in dividing two simulated distributions, the effects of minor imperfections of the used model cancel out. In the current studies only the energy regions where the overall efficiency changes monotonically are selected for the further analysis. The small fluctuations observed within the selected energy limits of the overall efficiency have been smoothed by applying a sliding average of three consecutive energy bins. The standard deviation of the sliding average is assigned as the systematic error of the overall efficiency. Its value varies in the range 2%–5%.

3. Sector

As explained in Sec. II, the HADES detection system consists of six equivalent sectors, which cover the forward emission cone and provide detection acceptance over the full azimuth angle ϕ. It was checked whether all sectors give equivalent contribution to the measured cross sections. For this purpose, the same kind of analysis as described above for the global setup has been performed for the particles detected in each individual sector. The differences are again dependent of the kind of detected particle, its energy, and the emission angle. The standard deviation of the average of results for individual sectors has been calculated for the selected particle, emission angle, and the energy bin. This value estimates the systematic uncertainty resulting from the differences in performance of individual sectors and is found to be below 7%.

The total systematic error squared is calculated as the quadratic sum of the uncertainty components discussed above. It is done for each particle type, selected emission angle $\theta \pm 1.5^\circ$ and for each energy bin (25 MeV) of the distribution.

IV. EXPERIMENTAL RESULTS

The high event statistics collected during the p (3.5 GeV) $+ {}^{93}$Nb run permits the determination of $d^2\sigma/d\Omega dE$ distributions for p, d, t, π^+, and π^- in the polar angular range from 20° to 80°.

All distributions for hydrogen isotopes are presented in Figs. 4–6, whereas the cross sections for charged pions are shown in Figs. 7 and 8. The experimental cross sections are plotted for the mean emission angles θ of 20°–80° in steps of 5° with spread of $\theta = \pm 1.5^\circ$. The presented values of cross sections are obtained for kinetic energy bins of 25 MeV size. The values of experimental errors are of the size of the marker and thus usually not visible in the plots. The constant normalization uncertainty of 15% is not included in the error bars shown in the plots. The insignificant statistical errors are neglected. Differences in the energy range for specific reaction

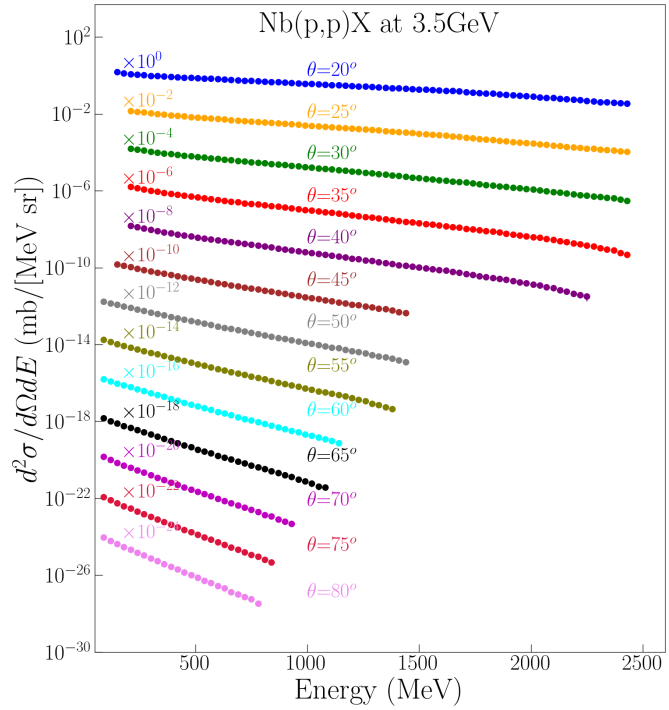

FIG. 4. Double-differential production cross sections of protons measured with HADES in p (3.5 GeV) $+ {}^{93}$Nb reactions (full circles). The distributions are scaled for better visibility. Statistical errors are negligible; for systematic errors see text.

products at different emission angles result from geometrical acceptance limits.

Exploiting the magnetic spectrometer component of HADES it was possible to register and identify the charged particles over a much broader energy range than accessible in earlier experiments designed for measurements of production cross section of light nuclear products. In fact, the energy range of the cross sections presented here in Fig. 4 clearly exceeds the energy limits of all proton distributions previously available in the literature.

The experimental double-differential cross sections of deuterons are limited in energy due the overlap of their dE/dx distributions with those of other hydrogen isotopes at higher particles energy. Still, our results (Fig. 5) on the cross section cover a wider range of energy than for deuteron data available up to now. The same holds for cross sections of tritons (Fig. 6).

The numerical values of the cross sections are available in the HEPData repository [60].

V. COMPARISON WITH WORLD DATA

From the particles of interest of the current study, only the negatively charged pions were examined in former analyses of HADES data collected for $p + {}^{93}$Nb reaction at 3.5 GeV [44]. It was checked that the current analysis provides almost identical distribution for the transverse momenta $p_\perp$ and the transverse mass $m_\perp$ as those published in Ref. [44].

Since other data for p (3.5 GeV) $+ {}^{93}$Nb reactions are not available in the literature, the data closest to the proton beam

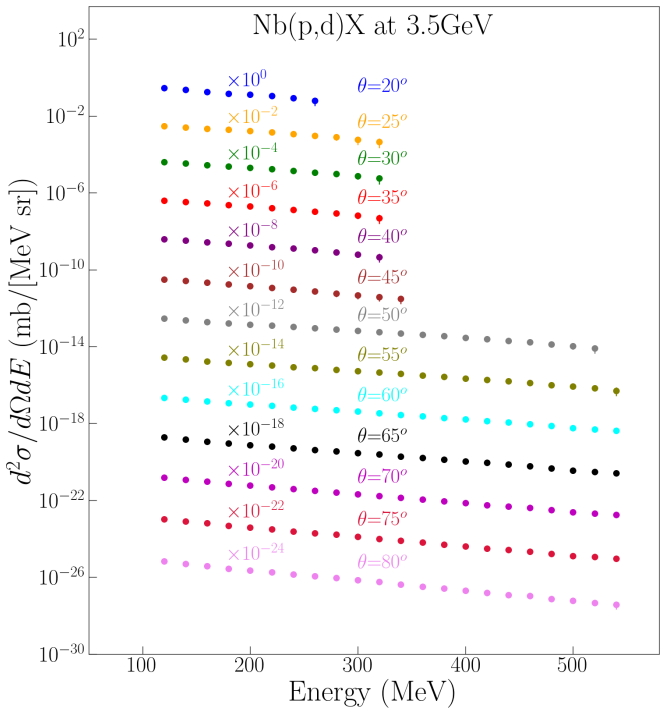

FIG. 5. The same as in Fig. 4 but for deuterons.

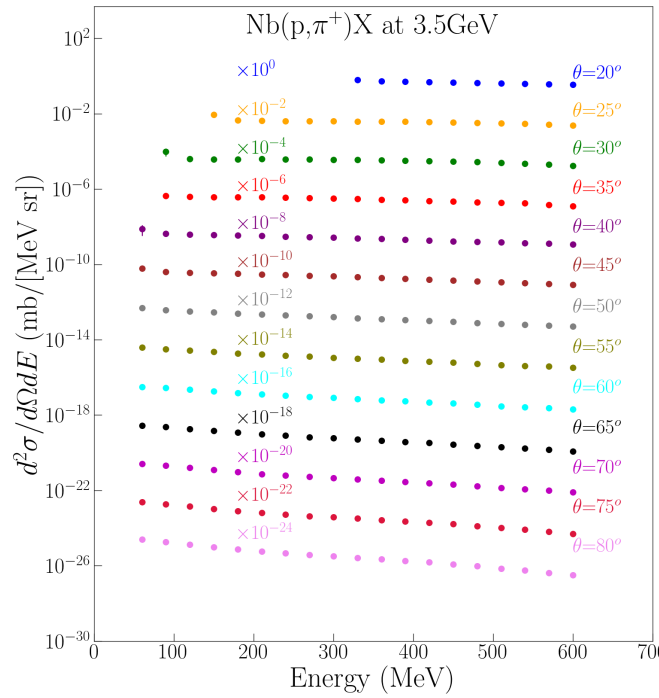

FIG. 7. The same as in Fig. 4 but for π^+.

energy and the target mass have been selected for the verification of the current results. The shapes of the spallation spectra in the energy and mass range of interest are independent of the target mass and the proton beam energy. The magnitude of the cross section rises with both the beam energy and the mass number A of the target. Since this rise is weak it allows for a comparison of the results for similar target masses and beam energies. Usually, the experimental uncertainties of the compared distributions are of similar order as the expected differences of the cross sections.

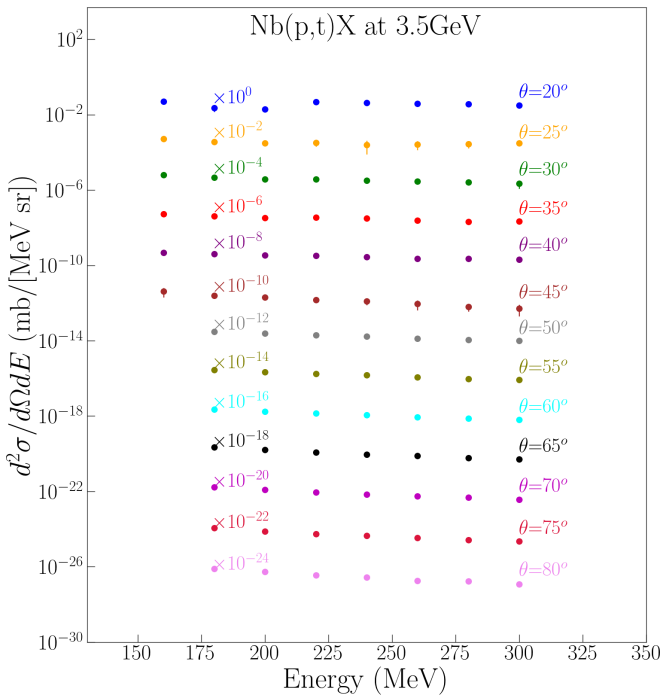

FIG. 6. The same as in Fig. 4 but for tritons.

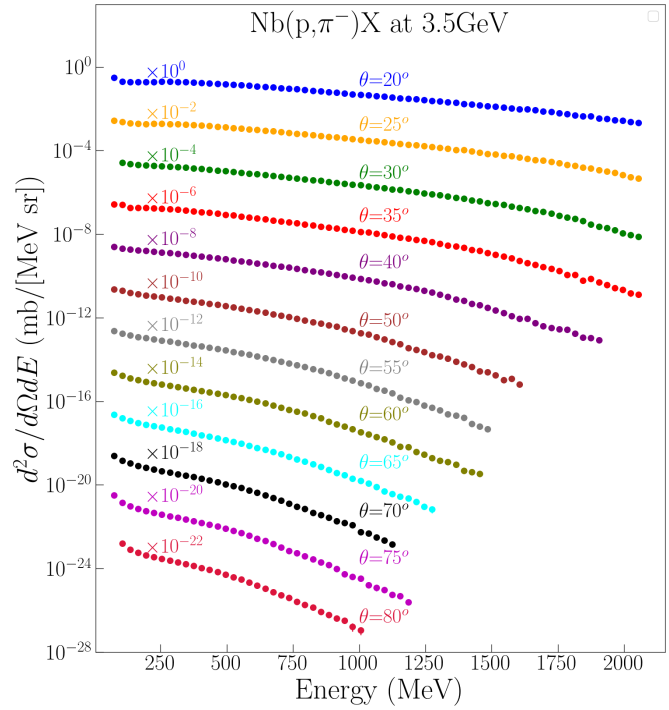

FIG. 8. The same as in Fig. 4 but for π^-.

A. Low-energy spallation data

The double-differential cross sections for light charged nuclear products were measured in a few dedicated experiments. Here a comparison is preformed with the results obtained for proton-nucleus collisions by the PISA and HARP-CDP collaborations. Data provided by PISA cover a broad range of target nuclei (from C to Au) bombarded by protons of 1.2, 1.9, and 2.5 GeV [32,33,36,37,61,62]. The HARP-CDP collaboration provided proton and pion spectra for proton induced reactions on some atomic nuclei from Be to Pb at 4.1 GeV proton bombarding energy [39,56–59,63–66].

In Fig. 9 the example of production cross sections for p (upper panel), d (middle panel), and t (lower panel) measured by the HADES collaboration for p (3.5 GeV) + ^{93}Nb and registered at a laboratory emission angle $\theta = 65^\circ$ are presented. The HADES results for protons are compared with the results by PISA measured for the reaction of $p + {}^{\text{nat}}$Ag at 2.5 GeV [33] and the results of HARP-CDP registered for $p + {}^{64}$Cu reactions at 4.1 GeV proton energy [58]. Taking into account the differences in beam energies, the results are in very good agreement. HADES deuteron and triton production cross sections are compared with the results by PISA collected for $p + {}^{\text{nat}}$Ag at 2.5 GeV reactions [33]. Here also a good agreement between HADES and PISA results is observed.

B. Midenergy pion spectra

The comparison of π^+ and π^- production with results by the HARP-CDP experiment is shown in Figs. 10 and 11, respectively. The HARP-CDP data were collected for a proton beam energy of 4.1 GeV and targets of ^{64}Cu [58] and ^{181}Ta [57]. The shapes of the energy distributions of π^+ measured at two angles (65° and 80°) are practically the same for all three targets. It is also the case for π^- measured at 35° and 55°. Since the proton beam energies in both experiments were similar, the measured cross sections were additionally divided by the corresponding target mass numbers. It could be concluded that, in the examined range of target masses and proton energies, the deviation from expected cross-section scaling with the target mass is lower than factor two. A good agreement of cross sections measured in both experiments is confirmed.

VI. COMPARISON WITH MODELS

It is reasonable to expect that the angular distribution of particles, emitted in forward direction as well as their energy distributions, contain information of the first stage of the proton-nucleus collision. This stage is referred to as an intranuclear cascade and is assumed to be a sequence of nucleon-nucleon and pion-nucleon interactions induced by the first collision of the projectile with one of the target constituents.

The obtained data provide a chance to extract important information on this stage of the collision, especially as the main charged participants of this process, pions and protons, are observed simultaneously in our experiment. They are accompanied with heavier hydrogen isotopes (d, t) with energies clearly higher than those typical for evaporated parti-

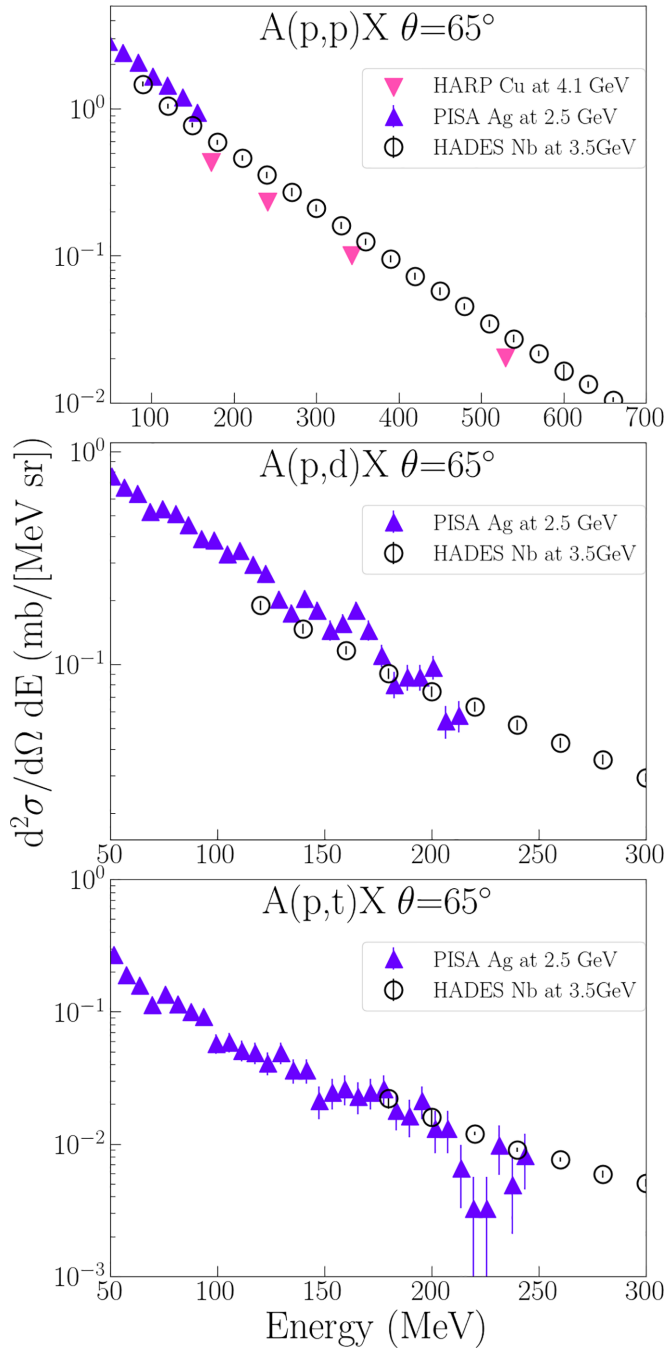

FIG. 9. Examples of double-differential cross sections for p (upper panel), d (middle panel), and t (lower panel) measured by HADES at $\theta = 65^\circ$ laboratory emission angle in p (3.5 GeV) + ^{93}Nb reactions. They are confronted with former results of the spallation experiment PISA [33] for the same isotopes and detection angle. The PISA data were measured with a $^{\text{nat}}$Ag target and for a proton beam energy of 2.5 GeV. The comparison results in a good agreement of the magnitudes and shapes of the distributions of both experiments. The double-differential production cross sections for p are also compared with the results obtained by the HARP-CDP experiment for the same detection angle, but for the reaction $p + {}^{65}$Cu at 4.1 GeV [58]. The small differences in the magnitudes of the p distributions of the various experiments are due to the expected target mass and proton beam energy dependence of the production cross section.

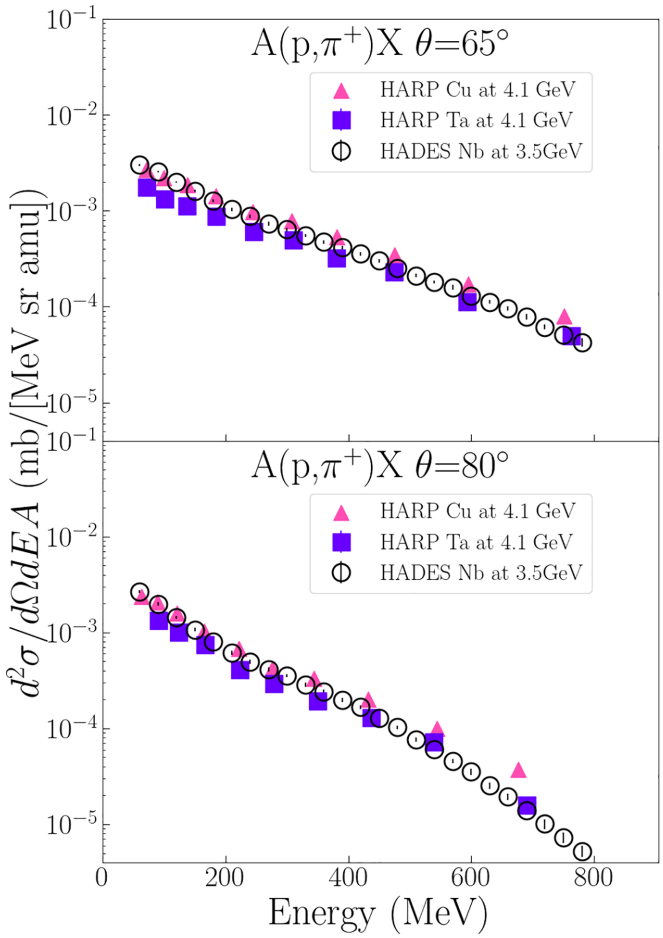

FIG. 10. Examples of double-differential cross sections measured at two emission angles ($\theta = 65°$, upper panel, and $\theta = 80°$, lower panel) by HADES for π^+ for p (3.5 GeV) + ^{93}Nb reactions. They are compared with similar results by the HARP-CDP collaboration measured for 4.1 GeV proton beam energy and targets of ^{64}Cu [58] and ^{181}Ta [57].

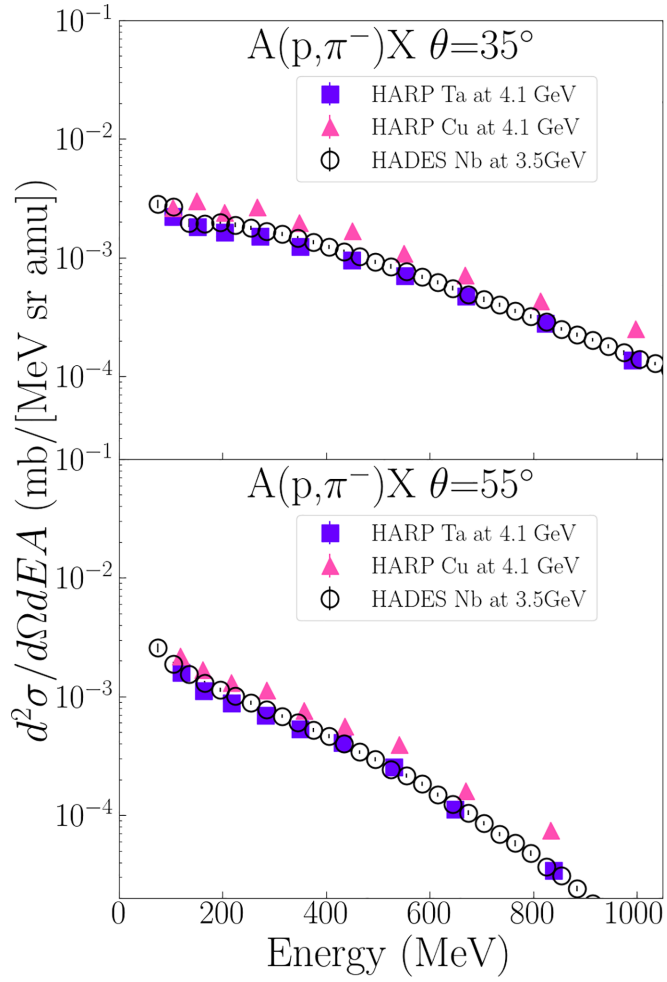

FIG. 11. Examples of double-differential cross sections measured at two emission angles ($\theta = 35°$, upper panel, and $\theta = 55°$, lower panel) by HADES for π^- for p (3.5 GeV) + ^{93}Nb reactions. They are compared with similar results by the HARP-CDP collaboration measured for 4.1 GeV proton beam energy and targets of ^{64}Cu [58] and ^{181}Ta [57].

cles. Thus, most probably the observed deuterons and tritons originate as well from the first stage of the reaction.

The experimental distributions are compared with the predictions of two models: GiBUU (release 2021, Feb 8, 2021) [42] and INCL++ (version v6.29-9198542) [29], which are commonly used in investigations of nucleus-nucleus collisions at GeV/A energies. The models differ in the level of approximation to the physical phenomena appearing in the quantum-mechanical realm of dynamical nuclear systems.

The Intranuclear Cascade Model of Liége (INCL++) [29] (and references therein) has been developed over the last four decades as a tool for simulations of spallation reactions. It employs a semiclassical treatment of the target nucleus and the nuclear cascade. An isospin and energy dependent nuclear mean field is assumed in which particle propagation proceeds along straight lines. Nucleon-nucleon as well as pion-nucleon collisions are probed stochastically. Their probability and the specific reaction channel depend on parametrized cross sections known from the interaction of free hadrons. INCL++ introduces basic quantum-mechanical prerequisites like the Pauli blocking or the tunneling probability of the Coulomb barrier by escaping particles from the interaction region.

Despite of its relative simplicity this model has significant advantages in comparison with other widely used models of such kinds of reactions: (i) Great attention is paid to the selection of parameters of the target nucleus. It concerns the density profile, diffuseness of the nuclear edge, the neutron skin and initial Fermi momentum distribution of nucleons. (ii) During the cascade the stability of the target nucleus is assured. The struck nucleus undergoes a mass loss due to emission of particles but the heavy remnant remains stable and does not blow up. (iii) For this reason, INCL++ allows us to calculate the properties of the reaction remnant. Its further fate can be credibly simulated by means of a statistical model. (iv) This model tries to explicitly introduce the dynamic creation of composite nuclear products by means of the so-called surface coalescence [21,23,29].

With the hypothesis of surface coalescence, the clustering is realized during the intranuclear cascade. The creation of

composite particles is tested when the single nucleon is going to be emitted. Then other nucleons of suitable isospin are searched for in its phase-space vicinity. Out of them the cluster is composed and, if the emission criteria for the new object are satisfied, it departs from the target nucleus.

In the Giessen Boltzmann-Uehling-Uhlenbeck project model (GiBUU), the multiparticle problem is discretized by the introduction of a statistically significant set of test particles for each simulated real particle instead of probing the continuous probability distributions of nuclear systems. Carefully constructed Hamiltonian and collision terms are used in order to simulate the evolution of the colliding system by solving transport equations. The time-dependent mean-field potentials—hadronic and electromagnetic—are included. As in other models, the geometrical cross sections (experimental or theoretical ones) for free hadrons are used in the calculation of the collision probability and its type. Pauli blocking is included for the collision output channel.

GiBUU is not equipped with mechanisms for the creation of composite particles. This is due to intrinsic limitations, namely, the difficulty to create density fluctuations in the distributions of the individual test particles.

Default settings were assumed for the GiBUU and INCL++ models for all numerical calculations performed in the present study.

A. Protons and pions

This section is devoted to angular and energy distributions of the main charged reaction products, namely, protons and charged pions. The light composite particles (deuterons and tritons), whose origin is much less understood, are considered afterwards. The cross sections presented here are given only for three detection angles, $\theta = 25^\circ$, 55°, and 80°, because the angular dependence of the data is monotonic and smooth. Furthermore, a selection of three energy spectra was done in order to facilitate the observation of certain trends of theoretical results which may differ for individual models and for various detection angles.

The uncertainties indicated for all presented experimental data include only the energy and angle-dependent components of the systematic uncertainties (see Sec. III D). The constant component of the uncertainty of 15%, resulting from absolute normalization factor, is not included in the plots. The insignificant statistical errors are neglected.

1. Protons

The obtained distributions, which are shown in Fig. 12, vary monotonically over the whole investigated energy range. Their slopes increase with the polar emission angle θ. A good agreement with the proton data at forward emission angles is provided by the GiBUU model. The theoretical curve follows the data for $\theta = 25^\circ$ in the whole presented energy range. The INCL++ model provides spectra of very similar shape as GiBUU but underestimates the magnitude of the data by a factor larger than two. The disagreement of the INCL++ model with the cross sections measured for protons is smallest at the lowest available energies and increases with increasing kinetic energy of the proton. Thus, the model distributions are steeper

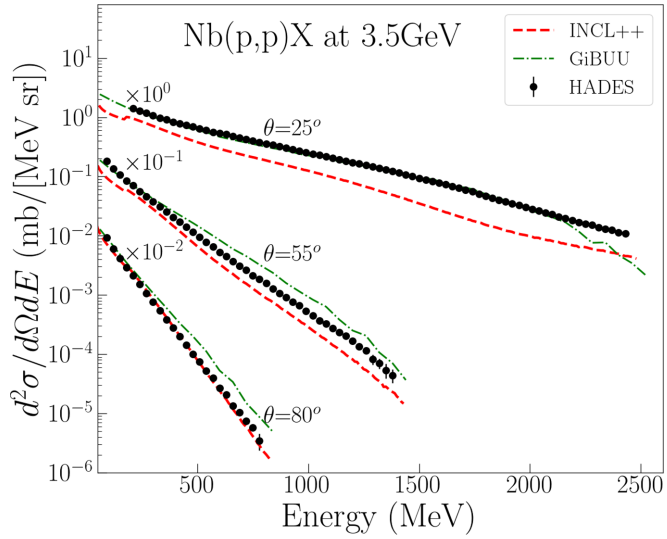

FIG. 12. Double-differential cross sections of protons measured by HADES in p (3.5 GeV) + ^{93}Nb reactions (full circles). Cross sections are shown for three laboratory emission angles $\theta = 25^\circ$, $\theta = 55^\circ$ (multiplied by factor 10^{-1}) and $\theta = 80^\circ$ (multiplied by factor 10^{-2}). The experimental distributions are compared with the results of two models: GiBUU (dash-dotted lines) and INCL++ (dashed lines). The constant normalization error of experimental data of 15% is not shown.

than the experimental curves. With increasing emission angle, GiBUU starts to overestimate the data, whereas the predictions of INCL++ get closer to the experimental distributions. For the highest angle, $\theta = 80^\circ$, a better description of the data is provided by INCL++, whereas GiBUU overestimates the experimental cross section. The discrepancy increases with the proton energy, attaining a factor $\approx$2 at the edge of available data range.

When comparing the predictions of GiBUU on proton production it has to be taken into account that this model does not include the formation of composite nuclear particles, which will affect the yield and kinematic distributions of protons.

2. Charged pions

At the most forward emission angles of π^+ (see Fig. 13) the model distributions underestimate the experimental cross sections at least by a factor of two. Only for higher particles energies above 500 MeV do results of GiBUU and INCL++ follow the data.

The agreement improves for larger emission angles. Both models follow approximately the shape of the experimental energy spectrum, being closest to the data in the pion energy range of 250–500 MeV. The models in general agree with the data within a factor of two.

At the highest detection angles presented here the BUU agrees with the data quite well. INCL++ underestimates the data by about a factor two or more in the low- and high-energy ranges.

From the comparison shown in Fig. 14 it can be concluded that GiBUU overestimates the data for all emission angles and energies of π^-. The discrepancies, except at the smallest

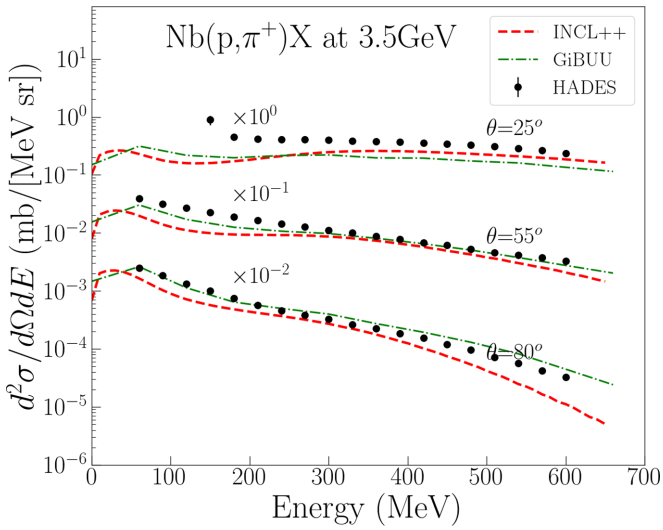

FIG. 13. The same as in Fig. 12 but for π^+.

energies, are at least a factor two. For larger emission angles INCL++ describes the data quite successfully, however, it fails for the lowest and highest energies of the detected pions.

B. Composite nuclear particles

Suitable mechanisms for the formation of composite nuclear products within an intranuclear cascade are not known. There are various hypotheses, which use more or less theoretically justified assumptions (see, e.g., Refs. [21,67–71]).

For low and medium energy pA reactions the most popular hypotheses are based on coalescence as the origin of composite particles during the prethermalization phase, at least for H and He isotopes. Unfortunately, among the tested models

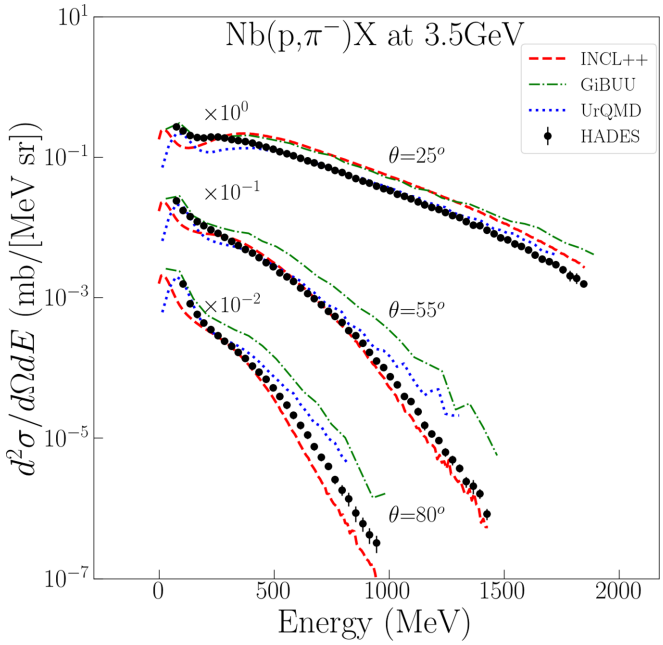

FIG. 14. The same as in Fig. 12 but for π^-.

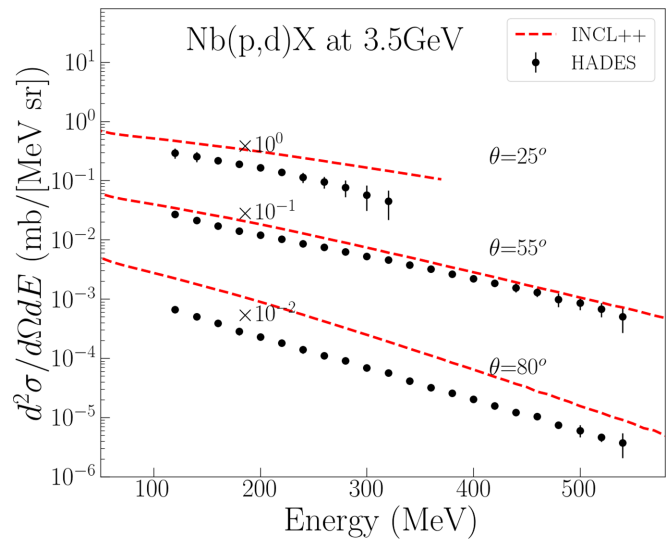

FIG. 15. Double-differential cross sections of deuterons measured by HADES in p (3.5 GeV) + ^{93}Nb reactions (full circles). Cross sections are shown for three polar laboratory emission angles of $\theta = 25°$, $\theta = 55°$ (multiplied by factor 10^{-1}) and $\theta = 80°$ (multiplied by factor 10^{-2}). The experimental distributions are compared with the results of INCL++ (dashed lines). The constant normalization uncertainty of 15% of the experimental data is not shown.

only INCL++ contains the mechanism of the so-called surface coalescence, which permits a dynamical construction of composite particles of masses $A \leqslant 8$. They can be emitted according to the conditions defined by the values of the binding energies and the height of the Coulomb barrier.

In kinetic transport models the creation of composite particles is modeled as well by coalescence in the final state. This is done by applying conditions on the mutual distances of nucleons in phase space after they are emitted from the target nucleus or after the freeze-out in heavy-ion collisions [72–75]. These methods do not contribute to the dynamics of intranuclear cascade and are therefore not considered in this work. Promising approaches are under development and are partially included, e.g., in the newest versions of the PHQMD [76] and SMASH [77] models but not in the GiBUU version used. We hope that the data presented help to further scrutinize those models.

In Figs. 15 and 16, the HADES results for deuterons and tritons, respectively, are confronted with the predictions by the INCL++ model. The surface coalescence model implemented in INCL++ generally overestimates the production of deuterons. For the forward emission angles of deuterons the slope of the theoretical curve is less steep than for the experimental distribution. With increasing energy of the emitted deuterons the discrepancy increases, reaching factors of $\approx$2.5 at energies >300 MeV. For higher emission angles the slopes of the theoretical distributions are the same as for the experimental ones. For $\theta = 55°$ the magnitude of cross sections differs by less than a factor two, whereas for $\theta = 80°$ it reaches already a factor of about four.

The limitations of the particle identification method based on the measurement of the dE/dx vs momentum dependen-

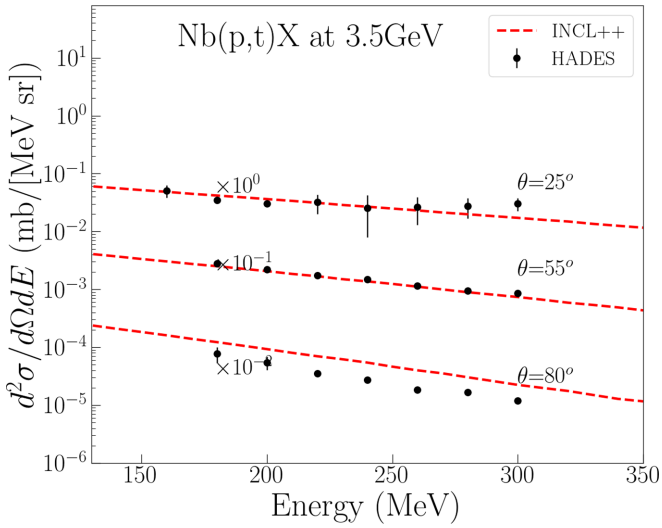

FIG. 16. The same as in Fig. 15 but for tritons.

cies have a strong effect on the accessible energy range for the triton cross sections. Nevertheless, as for the other hydrogen isotopes, it was possible to obtain distributions which extend in energy beyond earlier existing experimental data. The HADES results for triton are shown in Fig. 16. Astonishingly, the INCL++ model works better for the triton differential production cross sections than for deuterons. For tritons emitted at $\theta = 55^\circ$ the model curve agrees well with the experimental one over the whole measured energy range. Also for lower emission angles, the agreement of model and experiment is quite good with a slight underestimate of the experimental cross section at higher energies. Only at the highest angles measured by HADES, the model overestimates the experiment by a factor of two, whereas the slopes of experimental and model distributions are in good agreement.

VII. DISCUSSION OF RESULTS

In the previous section the comparison of the experimental spectra measured at three different angles with predictions of two models are discussed. It was found that the main properties of the data, such as a smooth decrease of the cross sections with increasing scattering angle and energy of the emitted particles, are reproduced by both models, while in detail there are discrepancies. It is evident that, for a closer investigation of the quality of the data reproduction by the models, additional measures useful for comparing data and models have to be involved. To perform a quantitative assessment of the models examined the method developed in Refs. [30,31] is applied. The application of so-called deviation factors is commonly used for the quantization of the validity of theoretical models, where conventional tools like the χ^2-squared test are not adequate for the studied problem. Various approaches were proposed for this purpose (see, e.g., Refs. [78–80]). A critical analysis of the applicability of various deviation factors to the cross section distributions typical for pre-equilibrium component of spallation reactions has been performed in Ref. [81]. For example, the popular H-deviation factor which, under some conditions, is equivalent to the χ^2 test is not applicable for the cases where both, the variation of the distributions and their uncertainties, are large. It was shown in Refs. [30,35,81] that for a validation of cross-section distributions in spallation physics the A-deviation factor is optimal. Hence, it is utilized here.

The deviation between two discrete distributions of cross sections can be quantified by a number between 0 and 1 defined by

$$A \equiv \frac{1}{N}\sum_{i=1}^{N}\frac{\left|\sigma_i^{\text{expt}} - \sigma_i^{\text{theor}}\right|}{\sigma_i^{\text{expt}} + \sigma_i^{\text{theor}}}, \tag{2}$$

where σ_i^{expt} and σ_i^{theor} are the values of the experimental and theoretical cross sections in the ith histogram bin, respectively, and N is the total number of histogram bins.

To give a consistent comparison of the models and the present data as a function of kinetic energy E of the reaction product, as well as its laboratory emission angle θ, the A quantity was calculated for each bin of the two-dimensional histograms θ vs E, i.e., without averaging over several bins [as done in Eq. (2)]:

$$A_i \equiv \frac{\left|(d^2\sigma/d\Omega dE)_i^{\text{expt}} - (d^2\sigma/d\Omega dE)_i^{\text{theor}}\right|}{(d^2\sigma/d\Omega dE)_i^{\text{expt}} + (d^2\sigma/d\Omega dE)_i^{\text{theor}}}, \tag{3}$$

where $(d^2\sigma/d\Omega dE)_i^{\text{expt}}$ and $(d^2\sigma/d\Omega dE)_i^{\text{theor}}$ are the values of experimental and theoretical differential cross sections for a given bin i in the 2D histogram of emission angle vs energy.

The quantity A vanishes ($A = 0$) for an ideal agreement, whereas its value increases with the deviation between the experimental and theoretical cross sections. Its highest possible value is equal to unity ($A = 1$) if one of the compared cross sections vanishes or if its value becomes infinite. In spite of such an asymmetrical behavior of A for large deviations between the compared cross sections, it has a very appealing property for small differences. Namely, the A values may be interpreted as the proxy of the half of the relative distance between the data and theoretical cross sections. For example, when $A = 0.1$ the average relative distance between experimental and theoretical cross sections is close to 20%, and for $A = 0.2$ the average deviation of the cross sections is close to 40%.

The total statistical and systematic uncertainties of the data presented in this work are usually below 20%. Thus, the resulting uncertainty of A remains below the value of 0.1.

Figure 17 presents the contour plots for A as a function of the particle's kinetic energy E and polar emission angle θ. It confirms to a large extent the conclusions derived from the qualitative analysis given in the previous section. In the upper set of the two panels of Fig. 17, representing proton data, the dark-blue and blue areas, where the discrepancy between data and model is smaller than 40%, are clearly larger for GiBUU than for INCL++. This proves that GiBUU results in a satisfactory agreement for a significantly larger number of angles and energies than INCL++. Moreover, the region of small values of A of INCL++ corresponds only to large

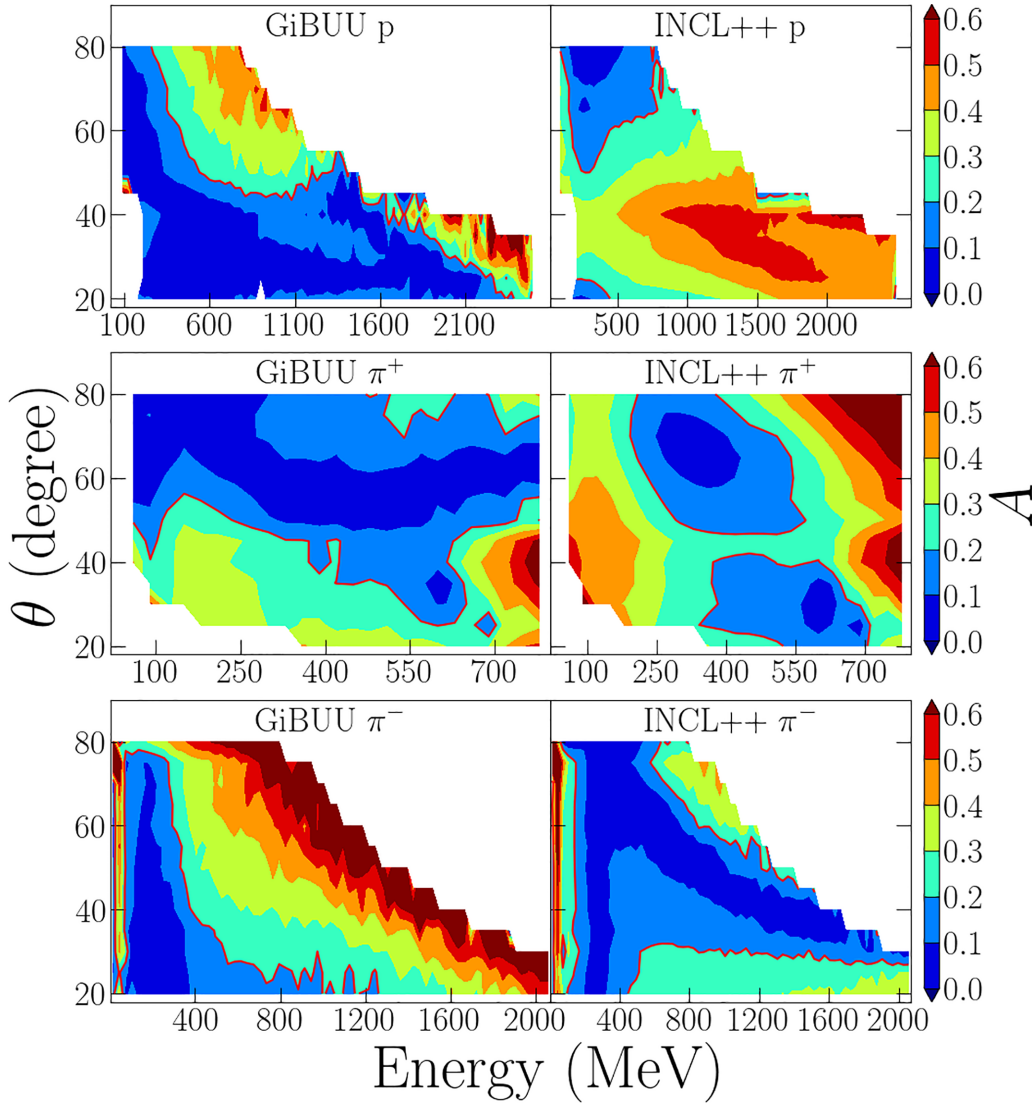

FIG. 17. Polar laboratory emission angle θ and kinetic-energy E-dependent distributions of the quantity A for p (upper row), π^+ (middle row), and π^- (lower row). It is calculated according to Eq. (3) for the GiBUU (left column) and INCL++ (right column) models in comparison with the experimental values of production cross sections measured with HADES. The kinematic regions, where data and model differ by less than 40% (i.e., $A \leqslant 0.2$), are plotted with blue and dark-blue colors and are surrounded by the red contour line. The uncertainty of A presented in this figure is below a value of 0.1. Note the different energy regions for the figures in different rows.

angles (larger than 50°) and relatively small energies (smaller than 1000 MeV), whereas GiBUU reproduces well the data at small angles (smaller than 50°) and at much broader ranges of energies for these angles, i.e., up to $E = 1500$–2000 MeV (depending on the scattering angle) but also at angles larger than 50°, albeit at the cost of smaller energy range (up to 400–500 MeV).

The middle two panels of Fig. 17 correspond to positively charged pions. It is evident that the regions of angles and energies well described by GiBUU cover angles larger than 50°, but the full range of pion energies (up to 800 MeV). The situation is different for the INCL++ model which describes satisfactorily well the data for almost all angles, however, in a limited range of energies from about 200 MeV to 500 MeV (at angles larger than 50°) and from about 300 MeV to 700 MeV (at angles smaller than 40°).

The lowest two panels of Fig. 17 represent the analysis of negatively charged pions π^- with the GiBUU and the INCL++ models (from the left to the right panel of the figure). It is clear that each of the models describes well different parts of the energy-angle plane: the GiBUU model reproduces the smallest fraction of the data. These data were reproduced for all angles, however, only for a small energy range, which decreases further when the emission angle increases. At the smallest angles (20°–25°), these energies belong to the interval from 100 to 600–700 MeV, whereas at the largest angles they lie in the interval from about 100 to 250 MeV. INCL++ describes well most of the π^- data. These data are mainly located at angles larger than 30° and cover a broad range of energies from 200 to 2000 MeV at 30°. This energy range decreases with increasing angle to the range 200 MeV to 650 MeV at the largest angle of 80°.

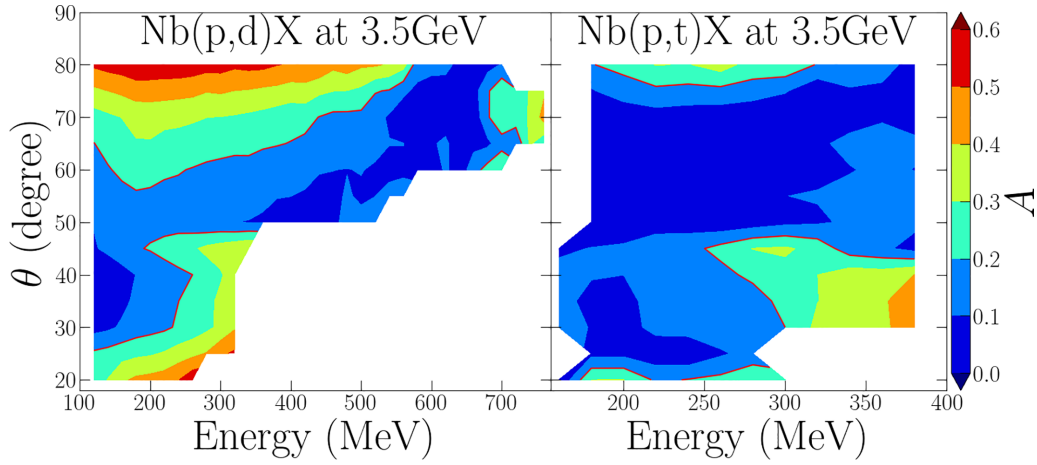

FIG. 18. Dependence of the A quantity on the deuteron (left panel) and triton (right panel) polar emission angle θ and kinetic energy E. The quantity A is calculated according to Eq. (3) to compare experimental double-differential cross sections measured by HADES with the results of the INCL++ model. The kinematic regions where data and model differ by less than 40% (i.e., $A \leqslant 0.2$) are plotted with blue and dark-blue colors and are surrounded by the red contour line. The uncertainty of A presented in this figure is below 0.1.

The data for the emission of deuterons and tritons can be compared only with predictions of the INCL++ model because GiBUU does not include a mechanism for cluster formation.

The A values for deuteron and triton production are presented in Fig. 18 in the form of two-dimensional maps showing the dependence on the isotope energy and polar emission angle. The behavior of A for deuterons indicates that discrepancies smaller than 40% may be expected for the full energy range only for angles about 50°–60°, while for tritons such an agreement is obtained for all angles larger than about 40° and additionally for energies smaller than approximately 270 MeV at angles smaller than 40°.

The quantity A allows us to characterize the predictive power of the used models. This is achieved by determining the fraction of studied two-dimensional space of energy-emission angle for which A values are smaller or equal to 0.2. The ratio of the number of these bins to the number of all observed bins can be used as a numerical measure of the predictive power (PP) of a given model for selected set of observed particles. The corresponding numbers for the INCL++ and GiBUU models are given in Table I.

VIII. SUMMARY

Experimental distributions of double-differential cross sections $d^2\sigma/d\Omega dE$ for p, d, t, π^+, and π^- production in p (3.5 GeV) + ^{93}Nb reactions have been extracted from data collected by a HADES experiment. The quality of the obtained cross sections has been verified by comparisons with other available experimental results published in the literature.

The data provided in this paper are measured in the angular range from 20° to 80° of the laboratory polar emission angle θ. Due to the high acceptance and the magnetic field of HADES the measured cross sections for almost all detected species and detection angles exceed the energy ranges of data available up

TABLE I. Measure of the predictive power (PP) of the GiBUU and the INCL++ models for double-differential cross sections of p, π^+, π^-, d, and t as measured by HADES. PP is equal to the fraction of the area (in [%]) of the θ vs E distributions presented in Figs. 17 and 18, where the agreement of the models and the experimental spectra of HADES is better than 20% ($A < 0.1$) or better than 40% ($A < 0.2$). PP for the simulation of the intranuclear cascade is given for the sum of p, π^+, and π^- ejectiles. The correctness of the reproduction of composite particle production is calculated for the sum of d and t (only for INCL++). The overall agreement of the INCL++ model with the data for all particles detected in HADES is given for the sum of them. The numbers corresponding to several emitted types of particles were calculated as the percentage of "good" bins for given set of particles among all bins corresponding to this set of particles.

	GiBUU		INCL++	
Ejectile	$A < 0.1$	$A < 0.2$	$A < 0.1$	$A < 0.2$
p	39%	65%	5%	19%
π^+	28%	58%	27%	35%
π^-	12%	28%	33%	63%
d			18%	52%
t			43%	76%
$d+t$			27%	60%
$p+\pi^++\pi^-$	26%	49%	16%	39%
$p+\pi^++\pi^-+d+t$			19%	43%

to now in the literature. The most significant extension of the measured kinematical region was obtained for proton data.

The obtained cross sections have been compared with the results of two reaction models, namely INCL++ and GiBUU. The comparison of the shapes and magnitudes of the experimental and theoretical cross sections show that, in general, these models are able to reproduce the data within a factor of two. Unfortunately, the correctness of the data description varies in a nontrivial way for each model with the type of produced particle, its energy and emission angle.

A quantitative comparison between data and model predictions is also done using the *A*-quantity, commonly employed for a comparison of spallative emission of slow particles with statistical models [30,31]. This comparison shows that a better description of the angular and energy dependent distributions of protons and charged pions is provided by the GiBUU model, whereas the accuracy of the description by INCL++ is by a factor of ≈1.5 worse.

The origin of energetic nuclear clusters (d and t) can be inferred from a comparison of the double-differential cross sections for the production of deuteron and triton registered in HADES with the results of the INCL++ model. The surface coalescence mechanism implemented in the INCL++ model as the source of light nuclei reproduces quite well the distributions of tritons. The modeled deuteron spectra overestimate however the data in the whole energy and angular range.

At the current stage of the theoretical examination of the dynamics of intranuclear cascades and the phenomena responsible for the clustering of nuclear matter in thermal preequilibrium, a clear conclusion about the validity of proposed scenarios cannot be drawn. The precision of the models is still not sufficient in order to perform a detailed verification of their features by a comparison to the experimental data. For example, the GiBUU model describes the p and π^+ spectra better than INCL++, but for π^- its results are worse than for the INCL++ model. GiBUU suffers as well from the lack of composite particle production. Introducing such a mechanism to this model would certainly modify also the theoretical p distributions. Thus, any judgments in favor of one of the two models tested here would be premature.

ACKNOWLEDGMENTS

The collaboration gratefully acknowledges the support by SIP JUC Cracow, Cracow (Poland), 2017/26/M/ST2/00600; TU Darmstadt, Darmstadt (Germany), VH-NG-823, DFG GRK 2128, DFG CRC-TR 211, BMBF:05P18RDFC1, HFHF, ELEMENTS 500/10.006, EMMI at GSI Darmstad; Goethe-University, Frankfurt (Germany), BMBF:05P12RFGHJ, GSI F&E, HFHF, ELEMENTS 500/10.006, HIC for FAIR (LOEWE), EMMI at GSI Darmstadt; JLU Giessen, Giessen (Germany), BMBF:05P12RGGHM; IJCLab Orsay, Orsay (France), CNRS/IN2P3; NPI CAS, Rez, Rez (Czech Republic), MSMT LTT17003, MSMT LM2018112, MSMT OP VVV CZ.02.1.01/0.0/0.0/18_046/0016066; WUT Warszawa (Poland) No: 2020/38/E/ST2/00019 (NCN), IDUB-POB-FWEiTE-3. We acknowledge the contribution from the following colleagues: G. Agakishiev, A. Belyaev, O. Fateev, A. Ierusalimov, V. Ladygin, T. Vasiliev, M. Golubeva, F. Guber, A. Ivashkin, T. Karavicheva, A. Kurepin, A. Reshetin, A. Sadovsky.

[1] https://www.psi.ch/en/sinq.
[2] https://www.isis.stfc.ac.uk.
[3] https://neutrons.ornl.gov.
[4] https://europeanspallationsource.se.
[5] http://english.ihep.cas.cn/csns/.
[6] http://j-parc.jp/MatLife/en/index.html.
[7] L. Medeiros-Romao and D. Vandeplassche, Conf. Proc. C **1205201**, 6 (2012).
[8] C. Rubbia, H. Ait Abderrahim, M. Björnberg, B. Carluec, G. Gherardi, E. Romero, W. Gudowski, G. Heusener, H. Leeb, W. von Lensa, G. Locatelli, J. Magill, J. Martinez-Val, S. Monti, A. Mueller *et al.*, The European Roadmap for Developing ADS for Nuclear Waste Incineration (2001).
[9] J. P. Meulders, A. Koning, and S. Leray, HINDAS - High and Intermediate Energy Nuclear Data for Accelerator-driven Systems. Detailed Final Report, Tech. Rep. (2005).
[10] Accelerator Driven Systems (ADS) and Fast Reactors (FR) in Advanced Nuclear Fuel Cycles, Nuclear Energy Agency - OECD (2002).
[11] E. Vangioni-Flam, M. Casse, and J. Audouze, Phys. Rep. **333-334**, 365 (2000).
[12] R. Ramaty, B. Kozlovsky, and R. E. Lingenfelter, Astrophys. J. **488**, 730 (1997).
[13] E. Vangioni-Flam and M. Casse, New Astron. Rev. **45**, 583 (2001).
[14] S. G. Mashnik, arXiv:astro-ph/0008382.
[15] K. Ammon, J. Masarik, and I. Leya, Meteorit. Planet. Sci. **44**, 485 (2009).
[16] E. Amato and P. Blasi, Adv. Space Res. **62**, 2731 (2018).
[17] R. Engel, D. Heck, and T. Pierog, Annu. Rev. Nucl. Part. Sci. **61**, 467 (2011).
[18] S. Mrówczyński, Eur. Phys. J. Spec. Top. **229**, 3559 (2020).
[19] A. Letourneau, J. Galin, F. Goldenbaum, B. Lott, A. Peghaire, M. Enke, D. Hilscher, U. Jahnke, K. Nunighoff, D. Filges, R. Neef, N. Paul, H. Schaal, G. Sterzenbach, and A. Tietze, Nucl. Instrum. Methods Phys. Res., Sect. B **170**, 299 (2000).
[20] S. Leray, F. Borne, S. Crespin, J. Frehaut, X. Ledoux, E. Martinez, Y. Patin, E. Petibon, P. Pras, A. Boudard, R. Legrain, Y. Terrien, F. Brochard, D. Drake, J. C. Duchazeaubeneix, J. M. Durand, S. I. Meigo, G. Milleret, D. M. Whittal, W. Wlazło *et al.*, Phys. Rev. C **65**, 044621 (2002).
[21] A. Letourneau, A. Böhm, J. Galin, B. Lott, A. Péghaire, M. Enke *et al.*, Nucl. Phys. A **712**, 133 (2002).
[22] A. Boudard, J. Cugnon, S. Leray, and C. Volant, Phys. Rev. C **66**, 044615 (2002).

[23] A. Boudard, J. Cugnon, S. Leray, and C. Volant, Nucl. Phys. A **740**, 195 (2004).

[24] M. G. Catanesi, E. Radicioni, R. Edgecock, M. Ellis, F. Soler, C. Gössling *et al.*, Phys. Rev. C **77**, 055207 (2008).

[25] L. Audouin, L. Tassan-Got, P. Armbruster, J. Benlliure, M. Bernas, A. Boudard *et al.*, Nucl. Phys. A **768**, 1 (2006).

[26] P. Napolitani, K. Schmidt, L. Tassan-Got, P. Armbruster, T. Enqvist, A. Heinz, V. Henzl, D. Henzlova, A. Kelic, R. Pleskac, M. V. Ricciardi, C. Schmitt, O. Yordanov, L. Audouin, M. Bernas, A. Lafriaskh, F. Rejmund, C. Stephan, J. Benlliure, E. Casarejos, M. Fernandez Ordonez, J. Pereira, A. Boudard, B. Fernandez, S. Leray, C. Villagrasa, and C. Volant, Phys. Rev. C **76**, 064609 (2007).

[27] L. Giot, J. Alcántara-Núñez, J. B. D. Pérez-Loureiro, L. Audouin, A. Boudard *et al.*, Nucl. Phys. A **899**, 116 (2013).

[28] T. Aoust and J. Cugnon, Phys. Rev. C **74**, 064607 (2006).

[29] A. Boudard, J. Cugnon, J.-C. David, S. Leray, and D. Mancusi, Phys. Rev. C **87**, 014606 (2013).

[30] S. K. Sharma, B. Kamys, F. Goldenbaum, and D. Filges, Eur. Phys. J. A **53**, 150 (2017).

[31] U. Singh, B. Kamys, F. Goldenbaum, D. Filges, Z. Rudy, and S. K. Sharma, Eur. Phys. J. A **54**, 109 (2018).

[32] A. Budzanowski, M. Fidelus, D. Filges, F. Goldenbaum, H. Hodde, L. Jarczyk *et al.* (PISA Collaboration), Phys. Rev. C **82**, 034605 (2010).

[33] M. Fidelus, D. Filges, F. Goldenbaum, L. Jarczyk, B. Kamys, M. Kistryn *et al.* (PISA Collaboration), Phys. Rev. C **96**, 064618 (2017).

[34] R. Serber, Phys. Rev. **72**, 1114 (1947).

[35] S. K. Sharma, B. Kamys, F. Goldenbaum, and D.Filges, Eur. Phys. J. A **52**, 171 (2016).

[36] A. Budzanowski, M. Fidelus, D. Filges, F. Goldenbaum, H. Hodde, L. Jarczyk, B. Kamys, M. Kistryn, S. Kistryn, S. Kliczewski, A. Kowalczyk, E. Kozik, P. Kulessa, H. Machner, A. Magiera, B. Piskor-Ignatowicz, K. Pysz, Z. Rudy, R. Siudak, and M. Wojciechowski (PISA Collaboration), Phys. Rev. C **80**, 054604 (2009).

[37] A. Bubak, A. Budzanowski, D. Filges, F. Goldenbaum, A. Heczko, H. Hodde *et al.* (PISA Collaboration), Phys. Rev. C **76**, 014618 (2007).

[38] M. Bonesini, Nucl. Phys. B, Proc. Suppl. **229-232**, 500 (2012).

[39] A. Bolshakova, I. Boyko, G. Chelov, D. Dedovitch, A. Elagin, D. Emelyanov, M. Gostkin, A. Guskov, Z. Kroumchtein, Y. Nefedov, K. Nikolaev, A. Zhemchugov, F. Dydak, J. Wotschack, A. De Min, V. Ammosov, V. Gapienko, V. Koreshev, A. Semak, Y. Sviridov *et al.*, Eur. Phys. J. C **72**, 1882 (2012).

[40] https://www-hades.gsi.de.

[41] G. Agakichiev *et al.* (HADES Collaboration), Eur. Phys. J. A **41**, 243 (2009).

[42] O. Buss, T. Gaitanos, K. Gallmeister, H. van Hees, M. Kaskulov, O. Lalakulich, A. B. Larionov, T. Leitner, J. Weil, and U. Mosel, Phys. Rep. **512**, 1 (2012).

[43] G. Agakishiev *et al.* (HADES Collaboration), Phys. Lett. B **715**, 304 (2012).

[44] G. Agakishiev *et al.* (HADES Collaboration), Phys. Rev. C **88**, 024904 (2013).

[45] G. Agakishiev *et al.* (HADES Collaboration), Phys. Rev. C **90**, 054906 (2014).

[46] G. Agakishiev *et al.* (HADES Collaboration), Eur. Phys. J. A **50**, 81 (2014).

[47] G. Agakishiev *et al.* (HADES Collaboration), Phys. Rev. Lett. **114**, 212301 (2015).

[48] J. Adamczewski-Musch *et al.* (HADES Collaboration), Phys. Rev. C **94**, 025201 (2016).

[49] G. Agakishiev *et al.* (HADES Collaboration), Eur. Phys. J. A **52**, 178 (2016).

[50] J. Adamczewski-Musch *et al.* (HADES Collaboration), Phys. Lett. B **781**, 735 (2018).

[51] D. R. Nygren, Converting vice to virtue: Can time-walk be used as a measure of deposited charge in silicon detectors? Internal LBL Note (1991).

[52] I. Kipnis, T. Collins, J. DeWitt, S. Dow, A. Frey, A. Grillo *et al.*, IEEE Trans. Nucl. Sci. **44**, 289 (1997).

[53] M. Sánchez, Ph.D. thesis, University of Santiago de Compostela, 2003 (unpublished).

[54] M. Lorenz, Ph.D. thesis, Johann Wolfgang Goethe University, 2012 (unpublished).

[55] P. Tlustý, M. Weber, and P. Salabura (HADES Collaboration), GSI Scientific Report (2010), p. 73.

[56] A. Bolshakova, I. Boyko, G. Chelov, D. Dedovitch, A. Elagin, D. Emelyanov, M. Gostkin, A. Guskov, Z. Kroumchtein, Y. Nefedov, K. Nikolaev, A. Zhemchugov, F. Dydak, J. Wotschack, A. De Min, V. Ammosov, V. Gapienko, V. Koreshev, A. Semak, Y. Sviridov *et al.*, Eur. Phys. J. C **62**, 697 (2009).

[57] A. Bolshakova, I. Boyko, G. Chelov, D. Dedovitch, A. Elagin, D. Emelyanov, M. Gostkin, A. Guskov, Z. Kroumchtein, Y. Nefedov, K. Nikolaev, A. Zhemchugov, F. Dydak, J. Wotschack, A. De Min, V. Ammosov, V. Gapienko, V. Koreshev, A. Semak, Y. Sviridov *et al.*, Eur. Phys. J. C **63**, 549 (2009).

[58] A. Bolshakova, I. Boyko, G. Chelov, D. Dedovitch, A. Elagin, D. Emelyanov, M. Gostkin, A. Guskov, Z. Kroumchtein, Y. Nefedov, K. Nikolaev, A. Zhemchugov, F. Dydak, J. Wotschack, A. De Min, V. Ammosov, V. Gapienko, V. Koreshev, A. Semak, Y. Sviridov *et al.*, Eur. Phys. J. C **64**, 181 (2009).

[59] A. Bolshakova, I. Boyko, G. Chelov, D. Dedovitch, A. Elagin, D. Emelyanov, M. Gostkin, A. Guskov, Z. Kroumchtein, Y. Nefedov, K. Nikolaev, A. Zhemchugov, F. Dydak, J. Wotschack, A. De Min, V. Ammosov, V. Gapienko, V. Koreshev, A. Semak, Y. Sviridov *et al.*, Eur. Phys. J. C **66**, 57 (2010).

[60] https://www.hepdata.net/.

[61] A. Budzanowski, M. Fidelus, D. Filges, F. Goldenbaum, H. Hodde, L. Jarczyk, B. Kamys, M. Kistryn, S. Kistryn, S. Kliczewski, A. Kowalczyk, E. Kozik, P. Kulessa, H. Machner, A. Magiera, B. Piskor-Ignatowicz, K. Pysz, Z. Rudy, R. Siudak, and M. Wojciechowski (PISA Collaboration), Phys. Rev. C **78**, 024603 (2008).

[62] M. Fidelus, D. Filges, F. Goldenbaum, H. Hodde, A. Jany, L. Jarczyk, B. Kamys, M. Kistryn, S. Kistryn, S. Kliczewski, E. Kozik, P. Kulessa, H. Machner, A. Magiera, B. Piskor-Ignatowicz, K. Pysz, Z. Rudy, S. K. Sharma, R. Siudak, and M. Wojciechowski (PISA Collaboration), Phys. Rev. C **89**, 054617 (2014).

[63] A. Bolshakova, I. Boyko, G. Chelov, D. Dedovitch, A. Elagin, D. Emelyanov, M. Gostkin, A. Guskov, Z. Kroumchtein,

Y. Nefedov, K. Nikolaev, A. Zhemchugov, F. Dydak, J. Wotschack, A. De Min, V. Ammosov, V. Gapienko, V. Koreshev, A. Semak, Y. Sviridov *et al.*, Eur. Phys. J. C **62**, 293 (2009).

[64] A. Bolshakova, I. Boyko, G. Chelov, D. Dedovitch, A. Elagin, D. Emelyanov, M. Gostkin, A. Guskov, Z. Kroumchtein, Y. Nefedov, K. Nikolaev, A. Zhemchugov, F. Dydak, J. Wotschack, A. De Min, V. Ammosov, V. Gapienko, V. Koreshev, A. Semak, Y. Sviridov *et al.*, Eur. Phys. J. C **70**, 573 (2010).

[65] A. Bolshakova, I. Boyko, G. Chelov, D. Dedovitch, A. Elagin, D. Emelyanov, M. Gostkin, A. Guskov, Z. Kroumchtein, Y. Nefedov, K. Nikolaev, A. Zhemchugov, F. Dydak, J. Wotschack, A. De Min, V. Ammosov, V. Gapienko, V. Koreshev, A. Semak, Y. Sviridov *et al.*, Eur. Phys. J. C **71**, 1719 (2011).

[66] J. H. Kang, Y. C. Qian, B. C. Li, and S. W. Wu, Adv. High Energy Phys. **2014**, 675192 (2014).

[67] P. Hodgson and E. Beták, Phys. Rep. **374**, 1 (2003).

[68] H. Iwamoto and Y. Uozumi, AIP Conf. Proc. **1005**, 140 (2008).

[69] D. Wei, N. Wang, and L. Ou, J. Phys. G **41**, 035104 (2014).

[70] K. Pysz, Phys. Rev. C **91**, 011602(R) (2015).

[71] S. Typel, G. Röpke, T. Klähn, D. Blaschke, and H. H. Wolter, Phys. Rev. C **81**, 015803 (2010).

[72] J. I. Kapusta, Phys. Rev. C **21**, 1301 (1980).

[73] B. Monreal, S. A. Bass, M. Bleicher, S. Esumi, W. Greiner, Q. Li, H. Liu, W. J. Llope, R. Mattiello, S. Panitkin, I. Sakrejda, R. Snellings, H. Sorge, C. Spieles, H. Stöcker, J. Thomas, S. Voloshin, F. Wang, and N. Xu, Phys. Rev. C **60**, 031901(R) (1999).

[74] L.-W. Chen, C. Ko, and B.-A. Li, Nucl. Phys. A **729**, 809 (2003).

[75] N. Sharma, T. Perez, A. Castro, L. Kumar, and C. Nattrass, Phys. Rev. C **98**, 014914 (2018).

[76] J. Aichelin, E. Bratkovskaya, A. Le Fèvre, V. Kireyeu, V. Kolesnikov, Y. Leifels, V. Voronyuk, and G. Coci, Phys. Rev. C **101**, 044905 (2020).

[77] J. Mohs, M. Ege, H. Elfner, and M. Mayer, Phys. Rev. C **105**, 034906 (2022).

[78] R. Michel, R. Bodemann, H. Busemann, R. Daunke, M. Gloris, H.-J. Lange, B. Klug, A. Krins, I. Leya, M. Lüpke, S. Neumann, H. Reinhardt, M. Schnatz-Büttgen, U. Herpers, T. Schiekel, F. Sudbrock, B. Holmqvist, H. Condé, P. Malmborg, M. Suter *et al.*, Nucl. Instrum. Methods Phys. Res., Sect. B **129**, 153 (1997).

[79] N. Kurenkov, V. Lunev, and Y. Shubin, Appl. Radiat. Isot. **50**, 541 (1999).

[80] A. Konobeyev, U. Fischer, A. Koning, H. Leeb, S. Leray, and Y. Yariv, J. Korean Phys. Soc. **5910**, 927 (2011).

[81] S. Sharma, Ph.D. thesis, Jagiellonian University, 2015 (unpublished).

Correction: The acknowledgment of contributions from colleagues was updated in agreement with APS editorial guidelines.